

CHEMICAL PHYSICS

Strong isotope effect in the VUV photodissociation of HOD: A possible origin of D/H isotope heterogeneity in the solar nebula

Zijie Luo^{1,2†}, Yarui Zhao^{2†}, Zhichao Chen^{2†}, Yao Chang², Su-e Zhang², Yucheng Wu², Jiayue Yang², Yi Cheng¹, Li Che¹, Guorong Wu², Daiqian Xie³, Xueming Yang^{2,4*}, Kaijun Yuan^{2,5*}

The deuterium versus hydrogen (D/H) isotopic ratios are important to understand the source of water on Earth and other terrestrial planets. However, the determinations of D/H ratios suggest a hydrogen isotopic diversity in the planetary objects of the solar system. Photochemistry has been suggested as one source of this isotope heterogeneity. Here, we have revealed the photodissociation features of the water isotopologue (HOD) at $\lambda = 120.8$ to 121.7 nm. The results show different quantum state populations of OH and OD fragments from HOD photodissociation, suggesting strong isotope effect. The branching ratios of H + OD and D + OH channels display large isotopic fractionation, with ratios of 0.70 ± 0.10 at 121.08 nm and 0.49 ± 0.10 at 121.6 nm. Because water is abundant in the solar nebula, photodissociation of HOD should be an alternative source of the D/H isotope heterogeneity. This isotope effect must be considered in the photochemical models.

INTRODUCTION

The provenance of water on Earth and other terrestrial planets has been discussed for a long time without reaching a consensus. Existing scenarios range from negligible to significant cometary contributions to terrestrial water (1–4). The current criterion to distinguish between different scenarios is determining the D/H ratios (e.g., the HOD/H₂O ratios) in the reservoirs for comets and Earth's oceans, because the D/H ratios provide clues for the formation and evolution of water in star-forming regions and, by comparison with cometary data, on the origin of water on Earth.

Measurements of D/H ratios in Oort cloud comet (OCC) water are highly variable (1.4×10^{-4} to 6.5×10^{-4}), with the lowest measured value being similar to the terrestrial ocean water [D/H = 1.5576×10^{-4} , Vienna standard mean ocean water) (5–9)]. The Jupiter family comets (JFCs) 103P/Hartley 2 and 45P/Honda-Mrkos-Pajdušáková have low water D/H ratios of 1.61 and less than 2.0×10^{-4} , respectively (10, 11), whereas the ROSINA mass spectrometer aboard the Rosetta spacecraft recorded a high D/H ratio (about three times that of Earth's oceans) in water vapor from 67P/Churyumov-Gerasimenko (12). This wide range of D/H ratios in JFC and OCC water precludes the cometary origin for the oceans (12). However, atmospheric processes, like isotopic exchange reactions (e.g., $\text{HOD} + \text{H}_2 \leftrightarrow \text{H}_2\text{O} + \text{HD}$) and photochemistry, may redistribute D/H ratio in water from the inner to the outer protoplanetary disc regions (13, 14). Isotopic exchange occurs rapidly at high temperatures in the inner regions of the disc and is sluggish at

low temperatures in the outer regions of the disc. Therefore, after the Sun's formation, the D/H ratio of water in the evolving protoplanetary disc would have been dependent on the temperature of the surrounding environment and distance from the Sun (15).

Photochemistry in the early solar nebula is regarded as an alternative source of isotopic fractionation (16). Isotope-selective photodissociation or self-shielding has been proposed for explaining the anomalous oxygen isotopic distributions observed among various early solar system objects that contain both ¹⁶O-rich and ¹⁶O-poor reservoirs (17–19). Self-shielding process happens when the solar radiation penetrates gaseous molecules (e.g., CO), which have isotope-dependent spectral line absorption and different isotopic abundances. Photochemical self-shielding may also be important in the photodissociation of water, because replacing hydrogen by deuterium leads to significant variations in absorption line positions and oscillator strengths of water (20–22). Besides the self-shielding effects, photodissociation processes of the water isotopologue (HOD) have also been believed to play an important role in determining the D/H ratio heterogeneity in the solar system. The current photochemical models have only concerned the photodissociation branching ratios of HOD, with assuming the same dissociation features for the H + OD and D + OH channels (7). The validity of this assumption, however, has not been experimentally proved yet.

Photodissociation of H₂O by solar vacuum ultraviolet (VUV) photons is known to be an important process in the solar nebula (23–26). Absorbing one photon at $\lambda \sim 160$ nm populates the lowest excited electronic ($\bar{A}^1\text{B}_1$) state of water; the subsequent direct dissociation from this state yields an H atom plus a ground state OH ($X^2\Pi$) radical with little internal excitation (27–30). Absorption to the second excited singlet ($\bar{B}^1\text{A}_1$) state maximizes at $\lambda \sim 128$ nm. This state displays a minor direct dissociation channel to the H + OH ($A^2\Sigma^+$) product and major indirect predissociation pathways via two conical intersections (CIs) with the ground ($\bar{X}^1\text{A}_1$) state potential energy surfaces (PESSs) at linear HOH and OHH configurations that favor formation of highly rotationally excited OH (X , $\nu = 0$)

¹Department of Physics, School of Science, Dalian Maritime University, 1 Linghai Road, Dalian, Liaoning 116026, China. ²State Key Laboratory of Molecular Reaction Dynamics and Dalian Coherent Light Source, Dalian Institute of Chemical Physics, Chinese Academy of Sciences, 457 Zhongshan Road, Dalian 116023, China. ³Institute of Theoretical and Computational Chemistry, Key Laboratory of Mesoscopic Chemistry, School of Chemistry and Chemical Engineering, Nanjing University, Nanjing 210093, China. ⁴Department of Chemistry, College of Science, Southern University of Science and Technology, Shenzhen 518055, China. ⁵University of Chinese Academy of Sciences, Beijing 100049, China.

*Corresponding author. Email: kjiuan@dicp.ac.cn (K.Y.); xmyang@dicp.ac.cn (X.Y.)

†These authors contributed equally to this work.

products (31–37). In addition, the higher electronic state (\bar{D}^1A_1) can be reached at around Lyman- α wavelength (121.6 nm). Dissociation from the \bar{D} state efficiently undergoes a fast conversion to the \bar{B} state surface via an avoided crossing at bent geometry (38, 39).

Studies of the HOD isotopomer show that the quantitative outcome of its dissociation is not the mean of those for H_2O and D_2O . Previous vibrationally mediated photodissociation of HOD with OD or OH bond preexcitation accessed different regions of the excited state PES, which leads to mode or isotopic selectivity (40–44). Recently, Harich *et al.* (45) studied the HOD photodissociation at 121.6 nm and found “extremely-rotationally excited” distributions in OH ($X, \nu = 0$) products. These states were slightly above the OH dissociation limit and were only supported through large centrifugal barriers. In another experiment (46), they revealed a strong population preference for OD ($A, \nu = 0, N = 28$), labeled as “single N phenomenon.” However, the isotope specific photodissociation features of HOD at a state-to-state level were not obtained thus far.

In this work, we have recorded the quantum state-resolved photodissociation features of HOD as well as the branching ratios of the H + OD and D + OH channels between 120.8 and 121.7 nm by using tunable VUV sources combined with the high-resolution H (D) atom Rydberg tagging time-of-flight (HRTOF) technique (47). The experimental results show that the quantum state population distributions of OD products differ markedly from that of OH products, revealing very strong isotope effect. This implies that an in-depth understanding of the OH (OD) product quantum state population patterns from photodissociation of HOD is an essential prerequisite for any quantitative photochemical modeling. The mechanisms for this isotope effect may be general for other molecules where indirect dissociation dynamics are involved.

RESULTS AND DISCUSSION

Photodissociation dynamics of HOD

The present photodissociation studies were performed on the HRTOF apparatus, which was equipped with a tunable VUV laser radiation source generated by the two-photon resonance-enhanced four-wave mixing scheme or by the VUV free electron laser (FEL) at the Dalian coherent light source (DCLS) (see Materials and Methods for more details). A pulsed supersonic molecular beam of HOD was crossed by the VUV photolysis laser beam, and the H (D) products were then detected by HRTOF technique. Because the HOD sample was made from the mixing of H_2O and D_2O samples, the H atoms can be formed from both H_2O and HOD and D atoms from both D_2O and HOD. In the measurement of H atom TOF spectra, the sample was made by mixing H_2O/D_2O volume ratio of 1:5, which yielded the estimated ratio of H_2O/HOD to be $\sim 1:9.5$ (fig. S1). The ratio in the molecular beam should be a little change due to different vapor pressures of HOD and H_2O at the same temperature. Nevertheless, the H atom signals from H_2O photodissociation were significantly suppressed and can be easily subtracted. The same strategy was used for D atom TOF spectra measurements by using the mixing ratio H_2O/D_2O of 5:1.

The H (D) atom TOF spectra from HOD photodissociation were recorded at several wavelengths between 120.8 and 121.7 nm. Knowing the distance traveled from the photodissociation region to the detector and the fragment masses, these TOF spectra can be converted into spectra of the total translational energy release (E_T). The E_T distributions obtained with the polarization vector ϵ_{phot} aligned

parallel and perpendicular to the detection axis can then be used to construct three-dimensional (3D) flux diagrams of the H + OD (D + OH) fragments. Figure 1 shows these 3D flux diagrams with a photolysis wavelength of 121.08 nm. Each diagram shows two groups of features: an inner group, associated with formation of levels of electronically excited A state of OH (OD) fragments, and an outer group, associated with ground X state OH (OD) products. It is interesting that the extremely tall features in Fig. 1B, which are attributable to OD (A) products, are not observed in the OH product features (Fig. 1A). These marked differences in the 3D distributions illustrate that the H + OD and D + OH channels may go through different dissociation pathways.

For detailed analysis and feature assignments, the E_T distributions in parallel and perpendicular directions at $\lambda = 121.08$ nm are plotted in Fig. 2. All of these E_T distributions show progressions of sharp peaks. Given that the total energy and linear momentum must be conserved in the photodissociation process, e.g., in the D + OH channel, we can write

$$h\nu + E_{\text{int}}(\text{HOD}) - D_0(\text{D-OH}) = E_T(\text{D} + \text{OH}) + E_{\text{int}}(\text{OH}) \quad (1)$$

where the internal energy (E_{int}) distribution of the OH fragments can be determined from the E_T distribution; h is Planck's constant, and D_0 is the dissociation energy (48). In the supersonic expansion, the water molecule is cooled down to very low temperature, suggesting $E_{\text{int}}(\text{HOD}) \approx 0$. On the basis of previous spectroscopic data on the OH molecule (49), all of the intense sharp features in the spectra obtained at $\lambda = 121.08$ nm (Fig. 2A) can be readily assigned to high rotational levels of OH ($X, \nu = 0$) and OH ($A, \nu = 0$) radicals. Vibrationally excited OH (X) products are also observable in these spectra but with much lower relative yields. This energy disposal is very similar to that observed when exciting H_2O at the Lyman- α wavelength (35). We have also recorded the E_T spectra for this channel at 121.57 nm (fig. S2). The very similar feature has been observed again, suggesting the common dissociation features for this channel in the wavelength region of 121.0 to 121.6 nm. The dissociation features for the D + OH channel can be highlighted as follows (Fig. 3): (i) OH ($X, \nu = 0$) is the most important single vibrational product channel, while vibrationally excited OH products with $\nu \geq 1$ comprise approximately half of the total OH (X) population; (ii) the OH ($A, \nu = 0$) product populates to the highest energetically accessible

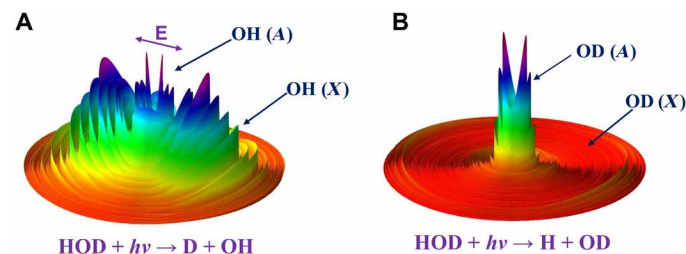


Fig. 1. The 3D product translational energy distributions. 3D contour plots of the (A) D + OH and (B) H + OD products from the photodissociation of HOD at 121.08 nm, with the translational energy up to $18,000 \text{ cm}^{-1}$. The double-headed arrow shows the alignment of photolysis laser, ϵ_{phot} . The outer rings in both plots are associated with formation of rovibrational states of the ground state OH/OD (X) radical products, while the inner structures are primarily due to OH/OD (A) products.

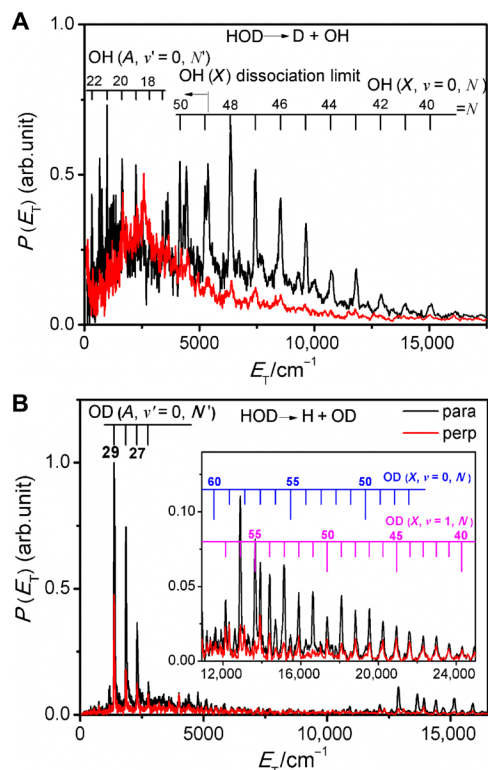


Fig. 2. The product translational energy distributions from HOD photodissociation. Translational energy spectra for the (A) D + OH and (B) H + OD products following photodissociation of HOD at 121.08 nm, with the detection axis parallel (black) or perpendicular (red) to the photolysis laser polarization, ϵ_{phot} . The inset in (B) displays the spectra in the high translational energy region. The sharp features can all be assigned to population of rovibrational states of OH/OD (X) and OH/OD (A). The OH (X) bond dissociation energy, D_0 (O–H), is also indicated in (A).

rotational levels and has strongly inverted rotational state distributions with the peak around $N = 21$.

In comparison with H_2O , a subtle difference can be observed. The rotational excitation of the OH ($X, v = 0$) product from HOD photodissociation is noticeably higher than that from H_2O [peaked at $N = 46$ (35)]. This can be directly attributed to the kinetic consequences of the difference in product masses. In H_2O , as the two H atoms start to accelerate away from the symmetrical Franck-Condon configuration, the developing translational energy will tend initially to be equally shared between them. One of these atoms dissociate, while the motion of the other will become internal energy of the OH product. In contrast, this sharing of the translational energy will tend to be two-thirds to the H atom and one-third to the D atom for HOD, leading to a higher internal energy of OH than that from H_2O and a lower internal energy of OD than that from D_2O . The strongest peak in the E_T spectra (Fig. 2A) is due to $N = 48$ level of OH ($X, v = 0$), and higher levels ($N = 49$ and 50) with significant populations can still be clearly observed. These extremely rotationally excited OH products have internal energy well above the OH bond dissociation limit, which have been labeled as “super rotors,” as reported by Harich *et al.* (45) and Chang *et al.* (50). The extremely high rotational excitation of the OH ($X, v = 0$) product had been attributed to dissociation through the HOH CI between the \bar{B} and \bar{X} state surfaces (45, 50). The dynamical similarity suggests that the

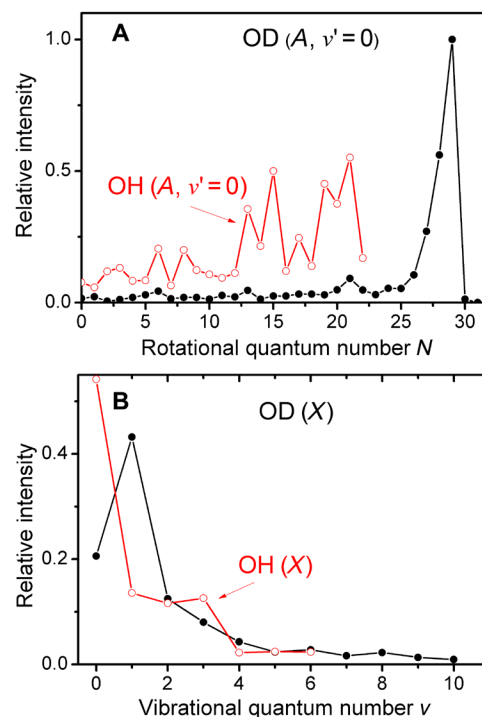


Fig. 3. The product quantum state population distributions from HOD photodissociation. (A) Rotational state population distributions of the OH/OD ($A, v' = 0$) and (B) vibrational state population distributions of the OH/OD (X) products formed in the photodissociation of HOD at 121.08 nm. The fitting spectrum for the D + OH channel did not contain the rotational levels for $v = 7$ to 10 due to a little relative resolution of the spectrum in the middle translational energy region shown in Fig. 2A.

D + OH channel from HOD photolysis around 121.0 to 121.6 nm also dominantly undergoes the HOD CI pathway between the \bar{B} and \bar{X} state surfaces, following the fast conversion from the initial excited \bar{D} state to the \bar{B} state (Fig. 4C).

In the case of the H + OD channel, however, the photodissociation features are markedly different. The structure assignment has been displayed in Fig. 2B. The striking phenomenon is extremely tall peaks at low translational energy, which are ascribed to the populations of OD ($A, v = 0, N = 27$ to 29) rotational levels. In particular, the intensity of the OD ($A, v = 0, N = 29$) state is almost 10 times larger than any other states except $N = 27$ and 28. The fitted rotational state population distributions of the OD ($A, v = 0$) are displayed in Fig. 3A. It is noted that more than 80% of OD (A) products populate in the three rotational levels $N = 27$ to 29. This abnormal rotational propensity has never been found in previous photodissociation of H_2O and D_2O and in the D + OH channel from HOD, to the best of our knowledge. This phenomenon can be seen in the whole wavelength region (120.8 to 121.7 nm) used in this work, and the E_T spectra at other five wavelengths have been shown in fig. S3. It is noted that the “single N propensity”—an extremely strong population for a single rotational state OD ($A, v = 0, N = 28$)—has also been observed at 121.68 and 121.43 nm (fig. S4), which is similar to that reported by Harich *et al.* (46) in the 121.6-nm HOD photodissociation. Another interesting phenomenon in this channel is that the OD ($A, v = 0$) product does not populate to the highest

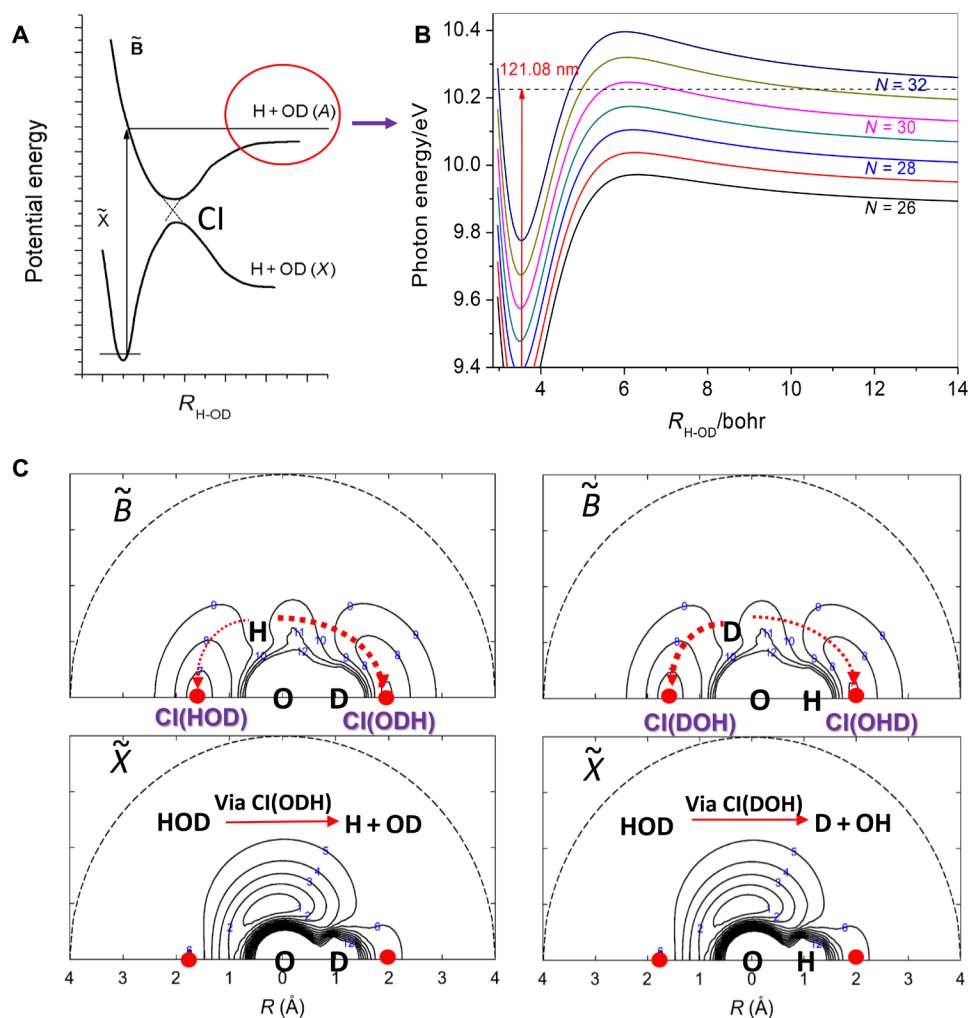


Fig. 4. The PESs of HOD and dissociation mechanism illustrations. (A) Schematic representation of HOD photodissociation at around 121 nm. (B) Adiabatic potential energy curves for the H + OD (A , $v = 0$, $N = 26$ to 32) system obtained by fixing the O-D bond. The rotational barrier is due to $N(N + 1)/(2\mu_{\text{R}}R^2)$ term in the Hamiltonian. The red arrow represents the excitation process, and the photon energy of 121.08 nm has been marked by a dotted line. (C) Contour plots of the \tilde{B} and \tilde{X} state PESs for the motion of H/D around OD/OH with a fixed OH/OD bond length of 1.07 Å. Energies are given in electron volts relative to the minimum of the ground state. The CIs at the linear HOD(DOH) and ODH(OHD) geometries, where minima of the \tilde{B} state PES are degenerate with maxima of the \tilde{X} state PES, are shown in red dots. The \tilde{B} and \tilde{X} state PESs correlate adiabatically with, respectively, H + OD (A) or D + OH (A) and H + OD (X) or D + OH (X) products. The red dotted curves in the top panel depict the dissociative flux through the two CIs, with a thicker pen thickness implying relatively larger yield. The inset panels show the pathways through the respective CIs.

energetically accessible rotational levels [$N_{\text{max}} = 31$ for OD (A , $v = 0$) at 121.08 nm], unlike the case for the D + OH channel.

The key to the understanding of the dissociation mechanism for this channel relies on the shape of the PES of the \tilde{B} state. As mentioned above, the initial excitation of water to the \tilde{D} state will fast convert to the \tilde{B} state, and on the \tilde{B} state, molecules undergo two main dissociation pathways: direct dissociation from this state to produce OD (A) products or indirect predissociation via nonadiabatic transfer from the \tilde{B} - \tilde{X} states at the two CI regions, yielding OD (X) products (Fig. 4A). The deep potential wells at CI regions force the hydrogen atom moving toward the linear geometry and get large amount of orbital angular momentum. For instance, when H atom moves toward the HOD CI (Fig. 4C), the OD molecule will rotate clockwise to compensate the change in angular momentum of the hydrogen atom. When N gets large, rotational barriers due to the $N(N + 1)/(2\mu_{\text{R}}R^2)$ term in the Hamiltonian significantly increase.

R is the internuclear distance, and μ_{R} is the reduced mass of the H-OD complex. In Fig. 4B, the adiabatic potential energy curves are shown for OD (A , $v = 0$) and for N levels between 26 and 32, obtained by fixing the O-D bond length of 2.04 bohr (close to the optimal OD distance with $v = 0$, $N = 28$). The photon energy at 121.08 nm is displayed with the dashed line. The state with $N = 31$ is actually an energetically accessible channel at 121.08 nm, but the rotational barriers for $N = 31$ and 30 prevent direct dissociation, which explains the observation of almost no population of $N > 29$ rotational levels.

When the hydrogen atom attempts to escape, the rotational barrier prevents dissociation, and the H atom returns to the OD molecule. The hydrogen atom would attempt several times to escape the OD molecule, and during each attempt, the torque modifies angular momenta for the OD and H motion, until finally N is low enough for the H atom to overcome the progressively smaller centrifugal barrier. This process leads to a strong preference for the formation

of OD fragments with the highest possible N value for which the barrier is low enough. Theoretical calculations (51) demonstrated that this abnormal rotational propensity can be interpreted in terms of dynamically constraint trajectories, i.e., trajectories that have turning points in the dissociation coordinate R due to the rotational barrier, rather than quantum interferences. Only the trajectories that pass the collinear ODH CI region with the R value in a specific narrow region will produce this strong rotational population propensity. This phenomenon is strongly energy-dependent and exclusively exists in the H + OD channel for HOD photodissociation around 121 nm.

The photodissociation feature of the H + OD channel in the high translational energy region is also different from that of the D + OH channel. At translational energy between 12,000 and 24,000 cm^{-1} , most of the sharp structures can be well assigned to rotational states of OD ($X, \nu = 1$), rather than OD ($X, \nu = 0$). The fitted vibrational state distributions of OD (X) products display that the OD ($X, \nu = 1$) is the dominant vibrational channel, while the vibrational ground state OD (X) products have only 20% population (Fig. 3B and fig. S5), in notable comparison with more than 50% OH (X) products in its ground vibrational state for the D + OH channel. The increased population of the vibrational excited OD products is a consequence of indirect predissociation from the ODH CI pathway (35). Dissociating molecules passing through the ODH CI will be temporarily trapped and make multiple jumps between the \bar{B} and \bar{X} state PESs, facilitating intramolecular vibrational redistribution between D-H and O-D vibrational motions that manifests OD (X) product vibrational excitation.

Thus, the cumulative evidence suggests that the H + OD channel from HOD photodissociation at around 121 nm mainly proceeds via the ODH CI pathway, whereas the D + OH channel at the same wavelength predominantly formed through the HOD(DOH) CI pathway (Fig. 4C). The different predissociation pathways cause the distinctive quantum state population distributions for the H + OD and D + OH channels, suggesting notably isotopic effects in the HOD photodissociation. The origin of this isotope effect is not immediately clear. Cheng *et al.* (52) demonstrated that the substitution in H_2O of one H by D leads to a rotation of the inertial axes by ca. 21° such that the H atom lies further away from the a -inertial axis than does the D atom by a factor of about 3.6. Hence, the rotational velocity of the H atom around the a axis will be 3.6 times greater than that of the D atom, which may force the H atom to easily access the linear ODH geometry.

Photodissociation branching ratios

As for the photodissociation process of HOD, branching ratios between the H + OD and D + OH channels have been an important “hotspot” for many theorists and experimentalist, not only because the ratios stimulate steering chemical reactions by the laser radiation but also because they directly relate to the D/H isotopic fractionation in the solar nebula. The theoretical calculations (40) predicted that the production of H + OD is favored over D + OH by a factor of 2.5, the value of which was usually used in the photochemical models (7). Experimentally, the branching ratios of the H and D products at 157.6 nm were separately estimated to be 4 ± 1 (53) and 2.46 ± 0.4 (27). In contrast, a ratio of 1.66 ± 0.50 in the 121.6-nm HOD photolysis has been reported (54), but the conclusion was questioned immediately by other researchers (55). These results showed that the photodissociation branching ratio of HOD is energy dependent and an accurate determination of the branching ratio is indispensable.

In this work, within the same experimental conditions, we have measured the total E_T distributions for the H + OD channel and the D + OH channel at 121.08 nm with the detection angle of 54.7° by using the VUV FEL laser (the magic angle; fig. S7). The detection efficiency of the H (D) RTOF technique has been calibrated by using the HD molecule dissociation. By integrating each rovibrational peak, the quantum yields for both channels can be obtained; thereby, their ratio will be considered to be the branching ratio. The ratio of φ [defined as (H + OD)/(D + OH)] is determined to be 0.70 ± 0.10 at 121.08 nm, notably different from the theoretical predictions (40) and previous experimental results (27, 53, 54). The branching ratio determined here is surprising because the OH bond fission propensity was expected, due to the OH bond [$D_0(\text{H-OD}) = 41,283 \pm 5 \text{ cm}^{-1}$] being weaker than the OD bond [$D_0(\text{D-OH}) = 41,751.3 \pm 5 \text{ cm}^{-1}$] (56). The probable reason is that in the nonadiabatic decay from the initial excited \bar{D} state to the \bar{B} state of HOD, there may be ample time for some vibrational modes to reach unexpected parts of the \bar{B} state surface, leading to dissociation dynamics different from starting according to a Frank-Condon-like transition. Previous experimental studies have also displayed the vibrationally mediated selective bond dissociation process of HOD, which leads to the large variation of the branching ratios [$\varphi(\text{H + OD})/(\text{D + OH}) = 0.08$ to 12] (40–44).

We have also measured the branching ratio of HOD photodissociation at 121.6 nm ($\varphi = \sim 0.49 \pm 0.10$, which means that the yield of D + OH products is about two times larger than that of H + OD products; see fig. S8). The result again shows the OD bond fission propensity, opposite to the theoretical prediction (40). It is obvious that the photodissociation branching ratio of HOD strongly varies with the photodissociation wavelength changing. This isotopic fractionation should also be considered in the photochemical models.

Potential relevance to the D/H isotopic fractionation in the solar system

Determination of the abundance ratios of the stable isotopes of the light elements, like D/H ratios, in different objects of the solar system provides important clues to the study of its origin and early history. Astronomical observations of the characteristic atomic and molecular emissions or absorptions from the interstellar space through ground- and/or space-based telescopes become the most important way to gain the isotopic abundance ratios in comets (15, 57). However, the D/H ratios returned by these measurements deviate significantly from Earth’s water D/H ratio, which brings back to the table the long-standing question whether or not water on Earth was delivered by comet impacts. Photochemistry has been accounted for in recent photochemical models for understanding the large isotopic fractionation effects that are apparent in carbon and oxygen in the solar system (58), which may also suit for understanding of the D/H isotope heterogeneity.

In this work, a notable quantum state-resolved isotope effect associated with the VUV photodissociation of HOD has been revealed. In the H + OD channel, dissociation via the linear ODH CI pathway between the \bar{B} and \bar{X} states leads to about 60% of OD products populating in the electronically excited state OD (A) (fig. S6), and most of which lie in the rotational levels ($\nu = 0, N = 27$ to 29). In comparison, in the D + OH channel, dissociation via the linear HOD CI pathway yields only $\sim 20\%$ of OH products in the OH (A) state with a wider range of rotational excitation. This cautions that the determination of the D/H isotopic ratios, which are based on the emission of the photofragments (like H/D Lyman- α or OH/OD A-X emission),

should involve this information in the photochemical modeling. It is noted that the rotational temperature of water at the expansion condition in this work is estimated to be about 10 K (36), which is close to the temperature of the interstellar medium. At higher temperatures, the water should populate to higher rotational levels. The dissociation features may be different because of rotational-specific predissociation dynamics.

The photodissociation branching ratios should also vary the cometary D/H isotopic ratio in water. The diatomic OH/OD fragments that resulted from these processes are highly excited with a lifetime of $\sim 1 \mu\text{s}$ (59) and are thus very chemically reactive. The subsequent ion- and/or neutral-molecule exchange reactions may redistribute the D/H ratios. Given that the total yields of $\text{HOD} \rightarrow \text{H} + \text{OD}$ plus $\text{D} + \text{OH}$ are equal to those of $\text{H}_2\text{O} \rightarrow \text{H} + \text{OH}$, $\text{HOD}/\text{H}_2\text{O} = (\varphi + 1)/\varphi \times (\text{OD}/\text{OH})$, where φ is the branching ratio of the $\text{H} + \text{OD}$ and $\text{D} + \text{OH}$ channels. It is noted that the D/H ratio is equal to half the HOD/ H_2O ratio, because water contains two atoms of hydrogen. Some models assume the ratio φ to be 2.5, adopted from previous theoretical calculations (40), which yields $\text{D}/\text{H} = \sim 0.7 \times (\text{OD}/\text{OH})$. In this work, the ratio φ around 121 nm is determined to be 0.70. This gives $\text{D}/\text{H} = \sim 1.2 \times (\text{OD}/\text{OH})$. This means that by adopting the branching ratio value from 2.5 to 0.70, the deduced D/H isotopic ratio increases about 70%. The quantitative assessment of these isotope effects needs to measure the photodissociation branching ratio of HOD in the entire solar VUV radiation region, and this is being performed in our laboratory. However, Lyman- α is the strongest line in the T Tauri phase of the Sun (60), the VUV flux of which in the early solar nebula is ~ 10 to 100 times higher than its neighboring wavelengths. The combination of the VUV flux and the absorption cross sections renders Lyman- α as the strongest contributor in the VUV photodissociation. Therefore, photodissociation of the HOD isotopomer and subsequent isotope exchange reactions may vary the D/H isotopic ratios in the inner and outer regions and/or in different periods of the solar nebula, which partly cause the D/H isotope heterogeneity in the solar system.

In summary, the quantum state-resolved dissociation features of the HOD photodissociation around 121 nm have been determined using tunable VUV sources in combination with the high-resolution H (D) RTOF technique. The distinctive quantum state populations of the $\text{H} + \text{OD}$ and $\text{D} + \text{OH}$ channels observed mainly stem from different predissociation pathways. The measurements also show that the branching ratios for the $\text{H} + \text{OD}$ and $\text{D} + \text{OH}$ channels vary with the photodissociation wavelengths. This extremely strong isotope effect in the photochemistry may affect the D/H isotope heterogeneity in the solar system and needs to be considered in the photochemical models.

MATERIALS AND METHODS

The HRTOF technique

The photodissociation of HOD was investigated using a recently developed VUV-VUV experimental scheme (61–63), using the HRTOF detection technique and a separate tunable VUV photolysis source. In the Rydberg tagging detection scheme, the H (D) atoms were excited from the ground state to a high Rydberg state via a two-step excitation: from the $n = 1$ to $n = 2$ states and then from $n = 2$ to a Rydberg state with principal quantum number $n \sim 45$. The first excitation step was achieved using coherent 121.6-nm radiation generated by difference four-wave mixing (DFWM) in a cell

containing a phase-matched Kr/Ar gas mixture and wavelengths of 212.5 nm (two photons of which are resonant with an excited state of atomic Kr) and 845 nm. The second excitation step required the absorption of one 365-nm photon, which was generated by doubling the output of a tunable dye laser operating at about 730 nm, pumped by the second harmonic of the Nd:YAG laser. The tunable photolysis source (in the range $120 \leq \lambda \leq 122$ nm) for these experiments was also generated by DFWM, using the same 212.5-nm radiation along with the output of another dye laser tunable in the range $810 \leq \lambda_T \leq 880$ nm. The polarization of the photolysis source could be changed by rotating the polarization of the λ_T laser using a set of half waveplates. The 121.6-nm radiation also induced photodissociation and generated H atom signals, so background subtraction was necessary. This was achieved by alternating the photolysis laser on and off, with the 121.6-nm intensity maintained as low as possible to maximize the relative tunable VUV laser-induced signal and to minimize the errors associated with the background subtraction process. The HOD sample was made by mixing H_2O and D_2O with the volume ratio of 1:5 or 5:1, and the Fourier transform infrared spectrum of which was shown in fig. S1. The HOD molecular beam was then generated by expanding the sample of 3% HOD in Ar. The Rydberg-tagged H (D) atoms were detected after TOF separation using a Z-stack microchannel plate detector, in front of which was a grounded fine mesh.

Photodissociation branching ratio measurement

The branching ratios of the $\text{H} + \text{OD}$ and $\text{D} + \text{OH}$ channels from HOD photodissociation at 121.08 and 121.6 nm were measured. The H atom TOF spectra and D atom TOF spectra at the magic angle (54.7°) were measured one by one in a few cycles, given the same experimental conditions for the two mixing samples in a short time. To gain large signals, the photolysis laser was generated by the VUV FEL at the DCLS (the VUV FEL radiation has a pulse duration of ~ 1.5 ps, a pulse energy of $> 100 \mu\text{J}/\text{pulse}$, and a spectral bandwidth of $\sim 50 \text{ cm}^{-1}$). To suppress the H atom background in the vacuum chamber, the gas pipe was cooled by liquid N_2 and the base vacuum of about 1×10^{-8} torr in the main chamber was achieved. The HD molecular beam was generated to calibrate the H (D) atom detection efficiency. The electron from an ion gauge dissociated HD to H and D atoms with the same amount. Extracting away the ions in the interaction region by a small electric field and subtracting the H atom background, the signal intensity of H atom and D atom from the H (D) TOF spectra should be same. The experimental results show that the HRTOF and the D atom Rydberg tagging time-of-flight (DRTOF) techniques have almost the same detection efficiency.

SUPPLEMENTARY MATERIALS

Supplementary material for this article is available at <http://advances.sciencemag.org/cgi/content/full/7/30/eabg7775/DC1>

REFERENCES AND NOTES

1. B. Marty, The origins and concentrations of water, carbon, nitrogen and noble gases on Earth. *Earth Planet. Sci. Lett.* **313–314**, 56–66 (2012).
2. C. M. O. Alexander, R. Bowden, M. L. Fogel, K. T. Howard, C. D. K. Herd, L. R. Nittler, The Provenances of asteroids, and their contributions to the volatile inventories of the terrestrial planets. *Science* **337**, 721–723 (2012).
3. N. Dauphas, The dual origin of the terrestrial atmosphere. *Icarus* **165**, 326–339 (2003).
4. T. Owen, A. Barnun, I. Kleinfeld, Possible cometary origin of heavy noble gases in the atmospheres of Venus, Earth and Mars. *Nature* **358**, 43–46 (1992).
5. H. Balsiger, K. Altwegg, J. Geiss, D/H and 18O/16O ratio in the hydronium ion and in neutral water from in situ ion measurements in comet Halley. *J. Geophys. Res.* **100**, 5827–5834 (1995).

6. P. Eberhardt, M. Reber, D. Krankowsky, R. R. Hodges, The D/H and $^{18}\text{O}/^{16}\text{O}$ ratios in water from comet P/Halley. *Astron. Astrophys.* **302**, 301–316 (1995).
7. D. Hutsemékers, J. Manfroid, E. Jehin, J. M. Zucconi, C. Arpigny, The $^{16}\text{OH}/^{18}\text{OH}$ and OD/OH isotope ratios in comet C/2002 T7 (LINEAR). *Astron. Astrophys.* **490**, L31–L34 (2008).
8. D. Bockelée-Morvan, N. Biver, B. Swinyard, M. de Val-Borro, J. Crovisier, P. Hartogh, D. C. Lis, R. Moreno, S. Szutowicz, E. Lellouch, M. Emprechtinger, G. A. Blake, R. Courtin, C. Jarchow, M. Kidger, M. Kuppers, M. Rengel, G. R. Davis, T. Fulton, D. Naylor, S. Sidher, H. Walker, Herschel measurements of the D/H and $^{16}\text{O}/^{18}\text{O}$ ratios in water in the Oort-cloud comet C/2009 P1 (Garradd). *Astron. Astrophys.* **544**, L15 (2012).
9. R. Meier, T. C. Owen, H. E. Matthews, D. C. Jewitt, D. Bockelée-Morvan, N. Biver, J. Crovisier, D. Gautier, A determination of the HDO/ H_2O ratio in comet C/1995 O1 (Hale-Bopp). *Science* **279**, 842–844 (1998).
10. P. Hartogh, D. C. Lis, D. Bockelée-Morvan, M. de Val-Borro, N. Biver, M. Kuppers, M. Emprechtinger, E. A. Bergin, J. Crovisier, M. Rengel, R. Moreno, S. Szutowicz, G. A. Blake, Ocean-like water in the Jupiter-family comet 103P/Hartley 2. *Nature* **478**, 218–220 (2011).
11. D. C. Lis, N. Biver, D. Bockelée-Morvan, P. Hartogh, E. A. Bergin, G. A. Blake, J. Crovisier, M. de Val-Borro, E. Jehin, M. Kuppers, J. Manfroid, R. Moreno, M. Rengel, S. Szutowicz, A Herschel study of D/H in water in the Jupiter-family comet 45P/Honda-Mrkos-Pajdušáková and prospects for D/H measurements with Ccat. *Astrophys. J. Lett.* **774**, L3 (2013).
12. K. Altwegg, H. Balsiger, A. Bar-Nun, J. J. Berthelier, A. Bieler, P. Bochsler, C. Briois, U. Gomboni, M. Combi, J. De Keyser, P. Eberhardt, B. Fiethe, S. Fuselier, S. Gasc, T. I. Calmanti, K. C. Hansen, M. Hassig, A. Jackel, E. Kopp, A. Korth, L. Leroy, U. Mall, B. Marty, O. Mouis, E. Neefs, T. Owen, H. Reme, M. Rubin, T. Semon, C. Y. Tzou, H. Waite, P. Würz, 67P/Churyumov-Gerasimenko, a Jupiter family comet with a high D/H ratio. *Science* **347**, 1261952 (2015).
13. L. Yang, F. J. Ciesla, C. M. O. Alexander, The D/H ratio of water in the solar nebula during its formation and evolution. *Icarus* **226**, 256–267 (2013).
14. C. Lecluse, F. Robert, Hydrogen isotope exchange reaction rates: Origin of water in the inner solar system. *Geochim. Cosmochim. Acta* **58**, 2927–2939 (1994).
15. L. J. Hallis, D/H ratios of the inner Solar System. *Philos. Trans. R. Soc. A* **375**, 20150390 (2017).
16. S. Chakraborty, T. L. Jackson, M. Ahmed, M. H. Thiemens, Sulfur isotopic fractionation in vacuum UV photodissociation of hydrogen sulfide and its potential relevance to meteorite analysis. *Proc. Natl. Acad. Sci. U.S.A.* **110**, 17650–17655 (2013).
17. R. N. Clayton, Self-shielding in the solar nebula. *Nature* **415**, 860–861 (2002).
18. H. Yurimoto, K. Kuramoto, Molecular cloud origin for the oxygen isotope heterogeneity in the Solar System. *Science* **305**, 1763–1766 (2004).
19. J. R. Lyons, E. D. Young, CO self-shielding as the origin of oxygen isotope anomalies in the early solar nebula. *Nature* **435**, 317–320 (2005).
20. K. J. Yuan, Y. Cheng, L. Cheng, Q. Guo, D. Dai, X. Wang, X. M. Yang, R. N. Dixon, Nonadiabatic dissociation dynamics in H_2O : Competition between rotationally and nonrotationally mediated pathways. *Proc. Natl. Acad. Sci. U.S.A.* **105**, 19148–19153 (2008).
21. B. W. Uselman, J. M. Boyle, S. L. Anderson, Multiphoton ionization vibrational state selection of H_2O^+ , D_2O^+ and HDO^+ . *Chem. Phys. Lett.* **440**, 171–175 (2007).
22. C. H. Yang, G. Sarma, J. J. ter Meulen, D. H. Parker, C. M. Western, REMPI spectroscopy and predissociation of the $\tilde{\text{C}}^1\text{B}_1(v=0)$ rotational levels of H_2O , HOD and D_2O . *Phys. Chem. Chem. Phys.* **12**, 13983–13991 (2010).
23. Y. Chang, Q. M. Li, F. An, Z. J. Luo, Y. R. Zhao, Y. Yong, Z. G. He, Z. C. Chen, L. Che, H. B. Ding, W. Q. Zhang, G. R. Wu, X. X. Hu, D. Q. Xie, J. M. C. Plane, W. H. Feng, C. M. Western, M. N. R. Ashfold, K. J. Yuan, X. M. Yang, Water photolysis and its contributions to the hydroxyl dayglow emissions in the atmospheres of Earth and Mars. *J. Phys. Chem. Lett.* **11**, 9086–9092 (2020).
24. Y. Chang, F. An, Q. M. Li, Z. J. Luo, L. Che, J. Y. Yang, Z. C. Chen, W. Q. Zhang, G. R. Wu, X. X. Hu, D. Q. Xie, K. J. Yuan, X. M. Yang, Electronically excited OH super-rotors from water photodissociation by using vacuum ultraviolet free-electron laser pulses. *J. Phys. Chem. Lett.* **11**, 7617–7623 (2020).
25. E. F. van Dishoeck, E. Herbst, D. A. Neufeld, Interstellar water chemistry: From laboratory to observations. *Chem. Rev.* **113**, 9043–9085 (2013).
26. J. S. Carr, J. R. Najita, The OH rotational population and photodissociation of H_2O in DG Tauri. *Astrophys. J.* **788**, 66 (2014).
27. X. F. Yang, D. W. Hwang, J. J. Lin, X. M. Ying, Dissociation dynamics of the water molecule on the $\tilde{\text{A}}^1\text{B}_1$ electronic surface. *J. Chem. Phys.* **113**, 10597–10604 (2000).
28. L. S. Zhou, D. Q. Xie, Z. G. Sun, H. Guo, Product fine-structure resolved photodissociation dynamics: The A band of H_2O . *J. Chem. Phys.* **140**, 024310 (2014).
29. I.-C. Lu, F. Y. Wang, K. J. Yuan, Y. Cheng, X. Yang, Nonstatistical spin dynamics in photodissociation of H_2O at 157 nm. *J. Chem. Phys.* **128**, 066101 (2008).
30. V. Engel, V. Staemmler, R. L. Vanderwal, F. J. Crim, R. J. Sension, B. Hudson, P. Andresen, S. Hennig, K. Weide, R. Schinke, Photodissociation of water in the first absorption band: A prototype for dissociation on a repulsive potential energy surface. *J. Phys. Chem.* **96**, 3201–3213 (1992).
31. D. H. Mordaunt, M. N. R. Ashfold, R. N. Dixon, Dissociation dynamics of H_2O (D_2O) following photoexcitation at the Lyman-Alpha wavelength (121.6 nm). *J. Chem. Phys.* **100**, 7360–7375 (1994).
32. L. S. Zhou, B. Jiang, D. Q. Xie, H. Guo, State-to-state photodissociation dynamics of H_2O in the B-band: Competition between two coexisting nonadiabatic pathways. *J. Phys. Chem. A* **117**, 6940–6947 (2013).
33. K. J. Yuan, R. N. Dixon, X. Yang, Photochemistry of the water molecule: Adiabatic versus nonadiabatic dynamics. *Acc. Chem. Res.* **44**, 369–378 (2011).
34. R. N. Dixon, D. W. Hwang, X. F. Yang, S. A. Harich, J. J. Lin, X. Yang, Chemical “double slits”: Dynamical interference of photodissociation pathways in water. *Science* **285**, 1249–1253 (1999).
35. S. A. Harich, D. W. H. Hwang, X. F. Yang, J. J. Lin, X. Yang, R. N. Dixon, Photodissociation of H_2O at 121.6 nm: A state-to-state dynamical picture. *J. Chem. Phys.* **113**, 10073–10090 (2000).
36. J. Bin, D. Q. Xie, H. Guo, State-to-state photodissociation dynamics of triatomic molecules: H_2O in the B band. *J. Chem. Phys.* **136**, 304302 (2012).
37. J. H. Fillion, R. van Harrevelt, J. Ruiz, N. Castillejo, A. H. Zanganeh, J. L. Lemaire, M. C. van Hemert, F. Rostas, Photodissociation of H_2O and D_2O in $\tilde{\text{B}}$, $\tilde{\text{C}}$, and $\tilde{\text{D}}$ states (134–119 nm). Comparison between experiment and ab initio calculations. *J. Phys. Chem. A* **105**, 11414–11424 (2001).
38. Y. Chang, J. M. Zhou, Z. J. Luo, Z. C. Chen, Z. G. He, S. R. Yu, L. Che, G. R. Wu, X. G. Wang, K. J. Yuan, X. M. Yang, Photodissociation dynamics of H_2O and D_2O via the $\tilde{\text{D}}^1\text{A}_1$ electronic state. *Phys. Chem. Chem. Phys.* **22**, 4379–4386 (2020).
39. K. J. Yuan, L. N. Cheng, Y. Cheng, Q. Guo, D. X. Dai, X. Yang, Two-photon photodissociation dynamics of H_2O via the $\tilde{\text{D}}$ electronic state. *J. Chem. Phys.* **131**, 074301 (2009).
40. J. Z. Zhang, D. G. Imre, OH/OD Bond breaking selectivity in HOD photodissociation. *Chem. Phys. Lett.* **149**, 233–238 (1988).
41. R. L. Vanderwal, J. L. Scott, F. F. Crim, Selectively breaking the O–H bond in HOD. *J. Chem. Phys.* **92**, 803–805 (1990).
42. R. L. Vanderwal, J. L. Scott, F. F. Crim, K. Weide, R. Schinke, An experimental and theoretical study of the bond selected photodissociation of HOD. *J. Chem. Phys.* **94**, 3548–3555 (1991).
43. H. Akagi, H. Fukazawa, K. Yokoyama, A. Yokoyama, Selective OD bond dissociation of HOD: Photodissociation of vibrationally excited HOD in the $\text{v}_{5,00}$ state. *J. Chem. Phys.* **123**, 184305 (2005).
44. S. Su, H. Z. Wang, Z. C. Chen, S. R. Yu, D. X. Dai, K. J. Yuan, X. Yang, Photodissociation dynamics of HOD via the $\tilde{\text{B}}^1\text{A}_1$ electronic state. *J. Chem. Phys.* **143**, 184302 (2015).
45. S. A. Harich, Y. F. Yang, X. M. Yang, R. N. Dixon, Extremely rotationally excited OH from water (HOD) photodissociation through conical intersection. *Phys. Rev. Lett.* **87**, 253201 (2001).
46. S. A. Harich, X. F. Yang, X. M. Yang, R. van Harrevelt, M. C. van Hemert, Single rotational product propensity in the photodissociation of HOD. *Phys. Rev. Lett.* **87**, 263001 (2001).
47. Y. Chang, Z. Chen, J. Zhou, Z. Luo, Z. He, G. Wu, M. N. R. Ashfold, K. Yuan, X. Yang, Striking isotopologue-dependent photodissociation dynamics of water molecules: The signature of an accidental resonance. *J. Phys. Chem. Lett.* **10**, 4209–4214 (2019).
48. O. V. Boyarkin, M. A. Koshelev, O. Aseev, P. Maksyutenko, T. R. Rizzo, N. F. Zobov, L. Lodi, J. Tennyson, O. L. Polyansky, Accurate bond dissociation energy of water determined by triple-resonance vibrational spectroscopy and ab initio calculations. *Chem. Phys. Lett.* **568**, 14–20 (2013).
49. J. S. A. Brooke, P. F. Bernath, C. M. Western, C. Sneden, M. Afsar, G. Li, L. E. Gordon, Line strengths of rovibrational and rotational transitions in the X^2TI ground state of OH. *J. Quant. Spectrosc. Radiat. Transf.* **168**, 142–157 (2016).
50. Y. Chang, Y. Yu, H. L. Wang, X. X. Hu, Q. M. Li, J. Y. Yang, S. Su, Z. G. He, Z. C. Chen, L. Che, X. Wang, W. Q. Zhang, G. R. Wu, D. Q. Xie, M. N. R. Ashfold, K. J. Yuan, X. Yang, Hydroxyl super rotors from vacuum ultraviolet photodissociation of water. *Nat. Commun.* **10**, 1250 (2019).
51. R. van Harrevelt, M. C. van Hemert, G. C. Schatz, A comparative classical-quantum study of the photodissociation of water in the $\tilde{\text{B}}$ band. *J. Phys. Chem. A* **105**, 11480–11487 (2001).
52. L. A. Cheng, K. J. Yuan, Y. Cheng, Q. Guo, X. M. Yang, R. N. Dixon, Product rotational Franck-Condon oscillations in HOD ($J_{\text{K}a\text{K}c}$) dissociation. *Mol. Phys.* **108**, 905–914 (2010).
53. N. Shafer, S. Satyapal, R. Bersohn, Isotope effect in the photodissociation of HDO at 157.5 nm. *J. Chem. Phys.* **90**, 6807–6808 (1989).
54. W. K. Yi, J. Park, J. Lee, Photodissociation dynamics of water at Lyman alpha (121.6 nm). *Chem. Phys. Lett.* **439**, 46–49 (2007).
55. P. Sharma, R. K. Vatsa, Comment on photodissociation dynamics of water at Lyman alpha (121.6 nm). *Chem. Phys. Lett.* **446**, 401–402 (2007).

56. L. N. Cheng, Y. Cheng, K. J. Yuan, Q. Guo, T. Wang, D. X. Dai, X. Yang, Photodissociation of HOD via the \tilde{C}^1B_1 state: OD/OH branching ratio and OD bond dissociation energy. *Chin. J. Chem. Phys.* **24**, 129–133 (2011).
57. D. Bockelee-Morvan, U. Calmonte, S. Charnley, J. Duprat, C. Engrand, A. Gicquel, M. Hassig, E. Jehin, H. Kawakita, B. Marty, S. Milam, A. Morse, P. Rousselot, S. Sheridan, E. Wirstrom, Cometary isotopic measurements. *Space Sci. Rev.* **197**, 47–83 (2015).
58. P. Jiang, X. P. Chi, Q. H. Zhu, M. Cheng, H. Gao, Strong and selective isotope effect in the vacuum ultraviolet photodissociation branching ratios of carbon monoxide. *Nat. Commun.* **10**, 3175 (2019).
59. D. R. Yarkony, A theoretical treatment of the predissociation of the individual rovibronic levels of OH/OD($A\ 2\Sigma^+$). *J. Chem. Phys.* **97**, 1838–1849 (1992).
60. M. W. Claire, J. Sheets, M. Cohen, I. Ribas, V. S. Meadows, D. C. Catling, The evolution of solar flux from 0.1 nm to 160 μm : Quantitative estimates for planetary studies. *Astrophys. J.* **757**, 95 (2012).
61. K. J. Yuan, L. N. Cheng, Y. Cheng, Q. Guo, D. X. Dai, X. M. Yang, Tunable VUV photochemistry using Rydberg H-atom time-of-flight spectroscopy. *Rev. Sci. Instrum.* **79**, 124101 (2008).
62. J. M. Zhou, Y. R. Zhao, C. S. Hansen, J. Y. Yang, Y. Chang, Y. Yu, G. K. Cheng, Z. C. Chen, Z. G. He, S. R. Yu, H. B. Ding, W. Q. Zhang, G. R. Wu, D. X. Dai, C. M. Western, M. N. R. Ashfold, K. J. Yuan, X. Yang, Ultraviolet photolysis of H_2S and its implications for SH radical production in the interstellar medium. *Nat. Commun.* **11**, 1547 (2020).
63. S. A. Harich, X. F. Yang, D. W. H. Hwang, J. J. Lin, X. Yang, R. N. Dixon, Photodissociation of D_2O at 121.6 nm: A state-to-state dynamical picture. *J. Chem. Phys.* **114**, 7830–7837 (2001).

Acknowledgments

Funding: The experimental work is supported by the Strategic Priority Research Program of the Chinese Academy of Sciences (grant XDB17000000), the Chemical Dynamics Research Center (grant 21688102), the National Natural Science Foundation of China (grants 21873099, 21922306, and 21773236), the Key Technology Team of the Chinese Academy of Sciences (grant GJJSTD20190002), the international partnership program of Chinese Academy of Sciences (grant 121421KYSB20170012), and Liaoning Revitalization Talents Program (grant XLYC1907154). **Author contributions:** K.Y. designed the experiments. Z.L., Y.Z., Z.C., Y.Cha., S.e-Z., Y.W. and Y.Che. performed the experiments. K.Y. and Z.L. analyzed the data. K.Y., J.Y., Y. Che, L.C., G.W., D.X., and X.Y. discussed the experimental results. K.Y., Z.L., and X.Y. prepared the manuscript. **Competing interests:** The authors declare that they have no competing interests. **Data and materials availability:** All data needed to evaluate the conclusions in the paper are present in the paper and/or the Supplementary Materials.

Submitted 28 January 2021

Accepted 4 June 2021

Published 21 July 2021

10.1126/sciadv.abg7775

Citation: Z. Luo, Y. Zhao, Z. Chen, Y. Chang, S.-e. Zhang, Y. Wu, J. Yang, Y. Cheng, L. Che, G. Wu, D. Xie, X. Yang, K. Yuan, Strong isotope effect in the VUV photodissociation of HOD: A possible origin of D/H isotope heterogeneity in the solar nebula. *Sci. Adv.* **7**, eabg7775 (2021).

Strong isotope effect in the VUV photodissociation of HOD: A possible origin of D/H isotope heterogeneity in the solar nebula

Zijie Luo, Yarui Zhao, Zhichao Chen, Yao Chang, Su-e Zhang, Yucheng Wu, Jiayue Yang, Yi Cheng, Li Che, Guorong Wu, Daiqian Xie, Xueming Yang and Kaijun Yuan

Sci Adv 7 (30), eabg7775.
DOI: 10.1126/sciadv.abg7775

ARTICLE TOOLS

<http://advances.sciencemag.org/content/7/30/eabg7775>

SUPPLEMENTARY MATERIALS

<http://advances.sciencemag.org/content/suppl/2021/07/19/7.30.eabg7775.DC1>

REFERENCES

This article cites 63 articles, 7 of which you can access for free
<http://advances.sciencemag.org/content/7/30/eabg7775#BIBL>

PERMISSIONS

<http://www.sciencemag.org/help/reprints-and-permissions>

Use of this article is subject to the [Terms of Service](#)

Science Advances (ISSN 2375-2548) is published by the American Association for the Advancement of Science, 1200 New York Avenue NW, Washington, DC 20005. The title *Science Advances* is a registered trademark of AAAS.

Copyright © 2021 The Authors, some rights reserved; exclusive licensee American Association for the Advancement of Science. No claim to original U.S. Government Works. Distributed under a Creative Commons Attribution NonCommercial License 4.0 (CC BY-NC).